42. O'Nions, R. K. & Pankhurst, R. J. *J. Petrol.* **15,** 603 (1974).
43. Mittlefehldt, D. W. & Wetherill, G. W. *Geochim cosmochim. Acta* **43,** 201 (1979).
44. Heymann, D., in *Handbook of Elemental Abundances in Meteorites* (ed. Mason, B.) (Gordon & Breach, Edinburgh, 1971).
45. Clarke, W. B., Jenkins, W. J. & Top, Z. *Int. J. app. Rad. Isotopes* **27,** 515 (1976).
46. Faure, G. & Powell, J. L. *Strontium Isotope Geology* (Springer, Berlin, 1972).
47. McColloch, M. T. & Wasserburg, G. J. *Science* **200,** 1003–1011 (1978).
48. Dasch, E. J. *Geochim. cosmochim. Acta* **33,** 1521–1552 (1969).
49. Hart, S. R. & Allegre, C. J. in *Physics of Magnetic Processes* (ed. Hargreaves, R.) 121–151 (Princeton University Press, 1980).
50. Voerwoerd, W. J. in *Marion and Prince Edward Islands* (eds Van Zinderen, E. M. *et al.*) (Balkema, Capetown, 1971).
51. Moore, J. G. *Am. J. Sci.* **263,** 40–52 (1965).
52. Moore, J., Claque, D. & Normark, W. *Geology* **10,** 88–92 (1982).

Scaling rules in rock fracture and possible implications for earthquake prediction

C. J. Allegre, J. L. Le Mouel & A. Provost

Institut de Physique du Globe, Université Paris 6, 2 place Jussieu, Paris 75005, France

A major preoccupation in physical sciences has been to interpret macroscopic events from microscopic phenomena. In some cases the change of scale is efficient and fairly easy to perform, but in others it turns out to be difficult and uninteresting. Success or failure is due more to the nature of the events than to the efficiency of the theoretical methods used. Some macroscopic phenomena have their origin in a microscopic organization which can be transferred to larger scales whereas others attain their structure on the macroscopic scale itself. Thus before applying scaling laws techniques[1–4] one must ensure that embedded scales are suggested by physical observations. That this seems to be the case for the fracture of rocks is supported by geological, seismological and rock mechanics observations. We have therefore built a very simple model based on scaling laws which yields a criterion for fragility at different scales and views rupture as a critical point. We use this model here to outline a general approach to earthquake prediction.

Fracturing occurs in rocks at all scales, from the microscale (microcracks) to the continental scale (megafaults), and the geologist can equally well observe embrittlement and rupture phenomena under the microscope as on satellite photographs (Fig. 1). But are the various scales of fracture related to one another? The following observations suggest they are: (1) field geologists know that the great faults of the crust—such as the San Andreas fault—actually consist of anastomosed faults, sometimes arranged *en échelon*, thus weakening a whole domain of the crust, down to variable depths[5]. (2) Seismologists who study source phenomena often have to introduce in their models complex rather than single faults, each one contributing to the observed radiation pattern[6,7]. (3) Rock mechanicists, when studying fracture in the laboratory, observe that it is preceded by the concentration of a swarm of microfissures which are themselves the result of an accumulation of microcracks[8–11]. From this set of observations one can suggest that fracture at the macroscopic scale is a consequence of accumulations of ruptures at lesser scales.

This hypothesis has been actually adopted by Brace and his students[8,9,11,12]. They have submitted rock samples to progressive triaxial loading ($\sigma_1, \sigma_2, \sigma_3$) and studied the increase of microcrack density with increasing load. This increase seems to be the result of two distinct processes: (1) the nucleation of new cracks, that is, the birth of new rupture points in the material; and (2) the growth of pre-existing cracks. In fact, as noted by Brace *et al.*[8] and Tapponnier and Brace[11], the nucleation seems to occur most often from a pre-existing crack. The distinction between the two processes is thus subtle and the increase in crack density can be considered to be ruled by a single phenomenon with a given activation energy.

The law governing the increase of microcrack density with deviatoric stress ($\sigma_1 - \sigma_3$) depends strongly on the confining pressure. But what seems to occur generally is that the macroscopic fracture is not preceded by an accelerated growth of microcrack density as measured over the whole sample. When the sample is examined at different scales one observes that cracks collect in some regions, but that these microscopic regions are roughly homogeneously distributed in the medium, even when the rupture threshold has been reached. On the other hand, the larger the scale the stronger is the spatial heterogeneity. The heterogeneity reaches, of course, a limit which determines the fracture itself whose orientation follows the laws established by Anderson[13].

We will now try to explain those observations with a simple renormalization group (RG) model and examine possible implications of the model for earthquake prediction.

For each elementary domain of rock (say 100 μm), we define two states: when the local microcrack density in the domain is greater than some critical value, it is considered as fragile (f); otherwise it is considered as sound (s).

As shown elsewhere (for example, see ref. 11), the mean microcrack density d depends linearly on $(\sigma_1 - \sigma_3)$ (for a given σ_2), but the local density varies considerably within the sample. The probability for an elementary domain to be fragile, p, is directly proportional to d and thus linearly related to $(\sigma_1 - \sigma_3)$ (for a given σ_2):

$$d = d_0 + b(\sigma_1 - \sigma_3)$$
$$p = ad = ad_0 + ab(\sigma_1 - \sigma_3) \quad (1)$$

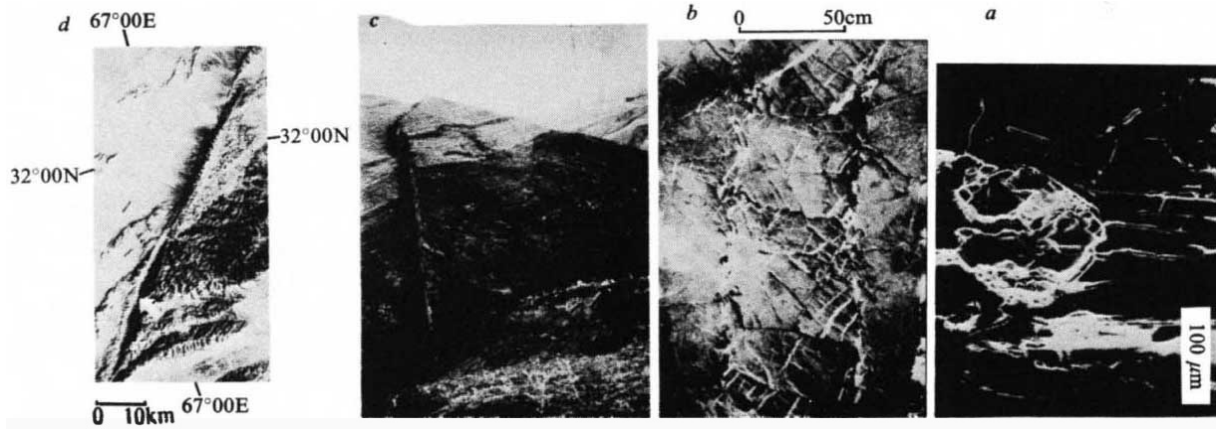

Fig. 1 Examples of fracture at different scales. *a*, Microcracks in quartz grains are induced by intense cracking in magnetite and plastic flow in biotite. (Westerly granite, fracture stress, 35 bar of confining pressure, room temperature.) *b*, Tension gashes, stylolites and micro shear faults in horizontal Mesozoic limestones (near Les Matelles, in Languedoc, France). The microstructures combine to form a fault zone at a larger scale. *c*, Master fault of the El Asnam, Algeria, earthquake (magnitude = 7.3, 10 October 1980). In the hills north of El Attaf, the break, several kilometres long, has up to 4 m of vertical throw. *d*, Landsat image of the Chaman strike-slip fault south-west of the Katawaz basin near the border between Afghanistan and Pakistan. The fault system, ~1,200 km long, may have accommodated as much as 500 km of left lateral displacement of India past Afghanistan in the past 40 Myr.

0028-0836/82/180047—03$01.00

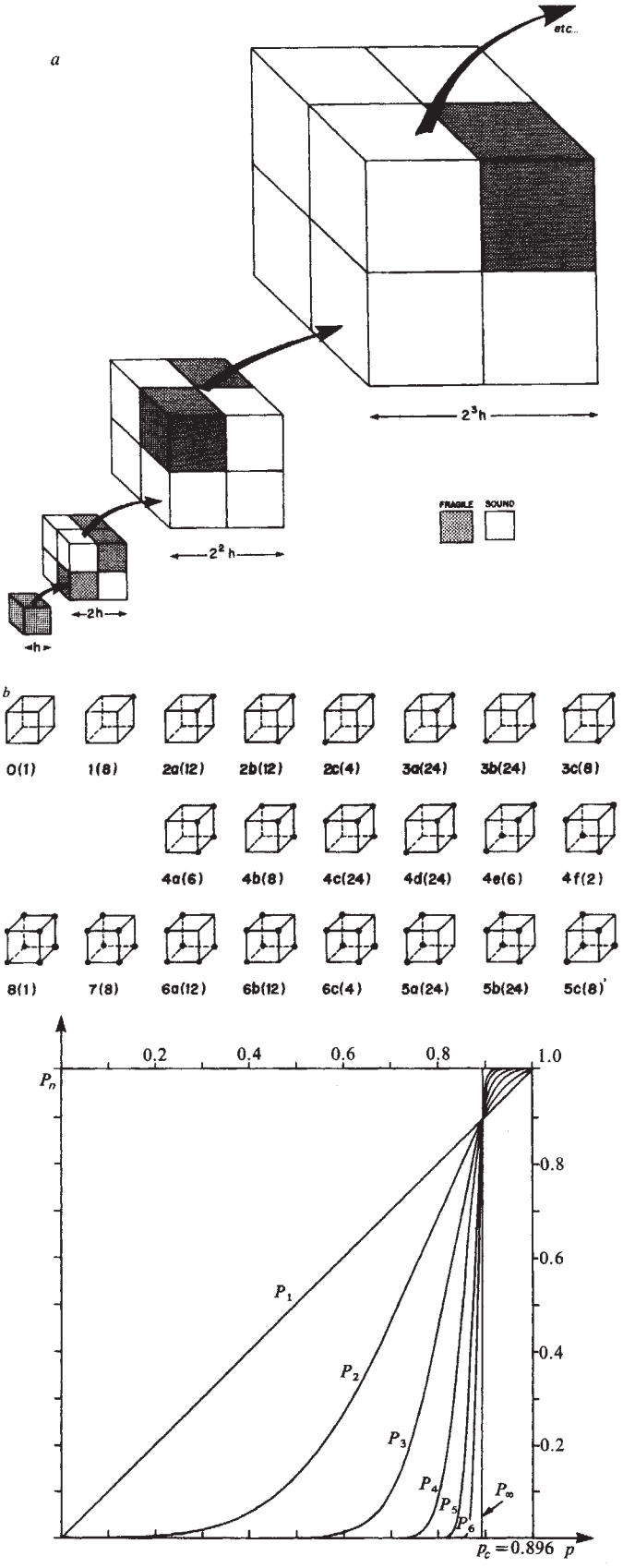

Fig. 2 *a*, Illustration of the renormalization group model. *b*, Now an *n*-order cube is depicted as a simple cube with its corners representing the eight constitutive $(n-1)$-order cubes. Each corner is marked by a solid dot when the corresponding $(n-1)$-order cube is fragile. This defines 22 configurations labelled 0, 1, 2a, ... 8 with their multiplicities in parentheses. The probability for a configuration with m corners fragile and multiplicity μ is: $\mu(P_{n-1})^m(1-P_{n-1})^{8-m}$. *c*, Probability P_n for an n cube being fragile plotted against the microscopic probability p.

Parameters d_0 and b depend on σ_2, whereas a can be considered purely geometrical.

Let us now develop a criterion for fragility at different scales. Let the elementary domain of order 1 be a cube of unit side (for example, 100 μm). Let the order of 2 cube be composed of 2^3 elementary order of 1 cubes, and so on (Fig. 2*a*).

In terms of $(n-1)$ cubes (we write n cube for the order of n cube), there are $2^8=256$ different n cubes. Taking the symmetry group of the cube into consideration, this number reduces to 22 topologically different configurations, each with a given multiplicity (Fig. 2*b*). An n cube will be considered sound whenever there is a 'pillar' of sound $(n-1)$ cubes that links two opposite faces. We thus consider as fragile the configurations labelled 4f, 5c, 6b, 6c, 7 and 8 in Fig. 2*b*. If P_n is the probability for an n cube being fragile, then:

$$P_1=p, \quad P_2=\Pi(p), \quad \ldots, \quad P_n=\Pi(P_{n-1}) \qquad (2)$$

with

$$\Pi(x)=2x^4(1-x)^4+8x^5(1-x)^3+16x^6(1-x)^2+8x^7(1-x)+x^8$$

The polynomial $\Pi(x)$ has the following simple properties: $\Pi(x)=x$ for $x=0$, $x=p_c=0.896$ and $x=1$. It monotonously increases with x on $[0, 1]$, being less than x on $]0, p_c[$ and greater than x on $]p_c, 1[$. Furthermore, $\Pi'(1)=\Pi'(0)=\Pi''(0)=\Pi'''(0)=0$. This explains the characteristics of the probability law P_n, which are illustrated in Fig. 2*c*. A striking feature is how rapidly the curves converge to the (Heaviside) step-function $H(p-p_c)$ with increasing n. For $n=5$, P_n positively jumps from 0 to 1 when p passes p_c.

This crude model allows one to account very simply for the observations of Tapponnier and Brace[11]. When counting microcrack density at the lowest scale an increase of this density increases with $(\sigma_1-\sigma_3)$ is observed, but nothing clearly announces the macroscopic rupture which appears as an 'exogen' discontinuity in a continuous process. The situation is quite different when looking at larger scales: little occurs before p gets to values close to p_c; then the fragility probability P_n jumps rapidly to values close to 1 and rupture occurs (see Fig. 3). p_c is thus a critical probability, the threshold for crack percolation.

Of course, the fragility criterion we have chosen is arbitrary and oversimplified. Other configurations of $(n-1)$ cubes may be supposed to make the n cube fragile. More refined criteria may be built by considering higher-order scaling steps ($3^3=27$, $4^3=64$, and so on, elementary cubes instead of $2^3=8$). In any case we get a recursion relationship between P_{n-1} and P_n of the form $P_n=\Pi(P_{n-1})$, Π being a polynomial with properties analogous to the ones above. Figure 4 illustrates a case in which the renormalization polynomial $\Pi(x)$ has no fixed point except the trivial ones $x=0$ and $x=1$. Although such a choice might seem inappropriate ($P_n\to 0$ when $n\to\infty$ for all $p<1$), it leads to the same conclusions (a step from very low to very high probabilities at the highest scales) due to the fact that there is

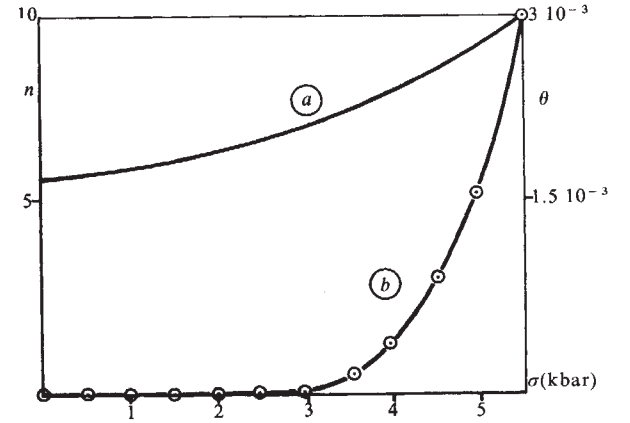

Fig. 3 Schematic representation of some experimental results (adapted from ref. 11). Sample of Westerly granite, confining pressure 500 bar. *a*, Variation with σ of a microscopic property (number of crack intersections/mm, n); *b*, variation with σ of a macroscopic property (volumetric crack dilatancy, θ).

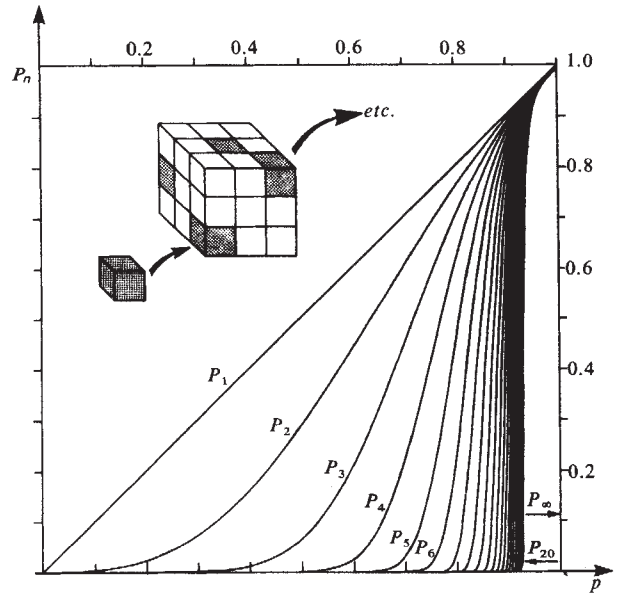

Fig. 4 Now an n cube, made of 27 $(n-1)$ cubes, is considered as fragile when three fragile $(n-1)$ cubes are aligned along one of the three medians of the n cube. Then $P_1 = p$, $P_2 = \Pi(p), \ldots, P_n = \Pi(P_{n-1})$ with $\Pi(x) = 3x^3 - 3x^5 + x^7$. With increasing n, the P_n curves sharpen rapidly to a quasi-step, then shift only slowly to the right. The last curve drawn is that for $P_{20}(3^{19} > 10^9)$. This shows that the prediction for megafaulting is not significantly altered by the mathematical absence of a critical probability p_c.

not an infinity of scaling steps from microcracks to megafaults (100 km/100 μm = 10^9). On the same basis it is also possible to build 'anisotropic models' in which the fragility is relative to a given direction and varies with this direction. But rather than generalizing, we will now draw some inferences about earthquake prediction from the simple model considered above.

The dilatancy theory for earthquake prediction which has been developed from laboratory experiments[8,14,15] has had some success but has failed to provide a general solution. Using a similar approach, we now show how to draw, from laboratory experiments, other useful inferences on earthquake prediction.

Earthquakes are fracture phenomena which most often occur on pre-existing sets of faults. Together with many theoretical seismologists we may assume that the reactivation of a fault system is a fracture phenomenon polarized by the existence of the fault itself[16,17]. Then the approach we propose, which determines a critical fragility, can also apply to earthquakes. One only needs to consider that the macroscopic domain with which our computations are concerned is the domain of the faults.

Earthquakes are probably generated by a strain accumulation under a constant deviatoric stress $\sigma = \sigma_1 - \sigma_3$ rather than by a continuous increase of σ with time. Mogi[18] has proposed that, in a medium submitted to a constant σ, the increase in the probability of occurrence of fracture during the time interval $(t, t+dt)$ does not depend on t and is given by $dp = \mu_0 \exp(\beta\sigma)\, dt$, where μ_0 and β are constants. We can also consider the more general case when stress is increasing with time:

$$p(t) = p_0 + \int_0^t \mu_0 \exp(\beta\sigma(t))\, dt \qquad (3)$$

(We may assume, in such conditions, that the microcrack density obeys a zero-order kinetic equation $d'(t) = \delta_0 \exp(\beta\sigma)$, $d(t)$ and $p(t)$ being related by $p(t) = a\, d(t)$, as above.)

It is then possible to compute the curves $P_n(t) = P_n[\sigma(t)]$ by the recursion formula (2). Of course, the shape of those curves is the same as that in Fig. 4, the parameter along the horizontal axis now being the time. For example, in the experiments of Kranz on samples of Barre granite[19], fracture occurs about 150 s after a stress of 2 kbar has been applied. To get the time parametrization, one has only to replace the $(0, p_c)p$ interval by a (0, 150 s) t interval. If σ is supposed to vary with time, a variable contraction or dilation of the horizontal axis can modify the figure of the $P_n(t)$ curves.

Suppose now we have two physical parameters, (x) and (y), which depend in a known way on crack density at different scales n_1 and n_2. It is then possible to predict the critical point $p(t) = p_c$ from the predicted intersection of the two curves $x(t)$ and $y(t)$. So it may be thought that the prediction of earthquakes demands the observation of phenomena characterized by different scales. For example, if one studies seismic waves for periods of 0.1, 1, 10, 100, ... s, one may think that the values of the corresponding attenuation ratios will tend towards some limit at the critical point (the partial failure of the (V_p/V_S) ratio prediction technique may come from the fact that in some circumstances this ratio depends on the scale but not in others, whether pores containing water in the rock are connected or not).

The crude model we propose here may be tested in two ways. First by studying in the laboratory the variation of crack density at different scales as $(\sigma_1 - \sigma_3)$ increases; second, by studying the variations of some physical properties which depend on crack density at different scales, especially in the vicinity of fracture.

Despite the extreme simplicity and the limits of our approach, if our basic conjecture is correct, a set of prediction methods could be built up.

We thank T. Madden, P. Tapponnier and V. Courtillot for fruitful discussion. P. Tapponnier provided the photographs in Fig. 1.

This is Institute de Physique du Globe contribution no. 578.

Received 6 January; accepted 11 March 1982.

1. Wilson, K. & Kogert, J. *Phys. Rep.* **12C**, 77 (1974).
2. Toulouse, G. & Pfeuty, P. *Introduction au Groupe de Renormalisation et à ses Applications* (Presse Université de Grenoble, 1975).
3. De Gennes, P. G. *Scaling Concepts in Polymer Physics* (Cornell University Press, 1979).
4. Madden, T. R. *Geophysics* **41**, 1104 (1976).
5. Mattauer, M. *Les Deformations de l'Écorce Terrestre* (Hermann, Paris, 1976).
6. Aki, K. *J. geophys. Res.* **84**, 6140 (1979).
7. Madariaga, R. in *Identification of Seismic Sources*, 71 (Reidel, Dordrecht, 1981).
8. Brace, W. F., Paulding, B. & Scholz, C. H. *J. geophys. Res.* **71**, 3939 (1966).
9. Waversik, W. R. & Brace, W. F. *Rock Mech.* **3**, 61 (1971).
10. Brace, W. F. & Bombolakis, E. G. *J. geophys. Res.* **68**, 3709 (1963).
11. Tapponnier, P. & Brace, W. F. *Int. J. Rock. Mech. Min. Sci. Geomech. Abstr.* **13**, 103 (1976).
12. Scholz, C. H., Sykes, L. R. & Aggarwal, Y. P. *Science* **181**, 803 (1973).
13. Anderson, E. M. *The Dynamics of Faulting and Dyke Formation with Applications to Britain* (Oliver & Boyd, Edinburgh, 2nd ed., 1951).
14. Scholz, C. H. & Kranz, R. *J. geophys. Res.* **79**, 2132 (1974).
15. Hadkey, B. *Proc. Conf. on Tectonic Problems at Low Confining Pressures* (ed. Nur, A.) 427 (CRL, Kovach, 1980).
16. Abe, K. *J. geophys. Res.* **79**, 4393 (1974).
17. Aki, K. *J. geophys. Res.* **73**, 5359 (1968).
18. Mogi, K. *Bull. Earth Res. Inst. Tokyo* **40**, 125 (1962).
19. Kranz, R. L. *J. Rock Mech. Min. Sci. Geomech. Abstr.* **16**, 23 (1979).

Cobalt in north-east Pacific waters

G. A. Knauer, J. H. Martin & R. M. Gordon

Moss Landing Marine Laboratories, Moss Landing, California 95039, USA

Significant understanding has been gained recently about the biogeochemical cycling of trace metals in the ocean. This knowledge has mostly resulted from the accurate measurement of dissolved species in oceanic water columns. We report here that cobalt's vertical distribution is similar to that exhibited[1-3] by Mn; that is, its surface enrichment/deep depletion (Fig. 1). However, amounts of Co (1–7 ng l^{-1}) are ~10–20 times less than those for Mn (Table 1), as might be expected from crustal abundance estimates[4] for these elements (Mn=950; Co = 25 μg per g). The similarity between Mn and Co profiles implies the same biogeochemical pathways. The Co excess in nearshore surface waters probably results from continental weathering input processes, as suggested by the remarkable Co–salinity mirror-image relationship shown in Fig. 1, and the Co–salinity scatter diagram in Fig. 2*a*. The steady decrease in Co concentrations also indicates that Co is usually scavenged rather than regenerated at depth, as is the case with Mn (Fig. 1; Table 1).

0028-0836/82/180049—03$01.00